

Full Length Research Paper

Estimation of gold mineralization using remote sensing techniques based on index calculation: Case of Betsiriry region, western Madagascar

Rakotondramano H.^{1,3*}, Razafindrakoto B.^{2,3} and Randriamiarantsoa T.⁴

¹Engineering and Geosciences, University of Antananarivo, Madagascar.

²Polytechnic School of Antananarivo, University of Antananarivo, Madagascar.

³Institute and Observatory of Geophysics of Antananarivo, Madagascar.

⁴Office of National Mines and Strategic Industries, Lalana Razanakombana Antananarivo 101, Madagascar.

Received 22 April, 2021; Accepted 14 June, 2021

It is undoubtedly true that the development of a country depends on the exploitation of these resources. In the case of Madagascar's Island, it is home to countless natural biological and mineral resources. Yet the island is underexplored, with most of the country's geological data dating from the 1950s. The use of modern technologies in mineral exploration and research facilitates and gives us many advantages. The time and investment cost will be less, but the results are reliable depending on the procedures to be followed in the processing, analysis and interpretation of the data acquired. By using ENVI software for ASTER and Landsat8 images, Index calculation of certain minerals, color composite and band ratio of the different spectral bands are the methods adopted to see the spatial distribution of gold deposits available in the study area located in the Betsiriry region in the western part of Madagascar. Field survey for verification is always recommended after software treatment, data analyses and interpretation.

Key words: Geographic information system (GIS), remote sensing, gold, betsiriry, index calculation.

INTRODUCTION

Satellite remote sensing images have been widely and successfully used for mineral exploration since the launch of Landsat in 1972. Gold is one of the most important mineral commodities that have been searched with the use of satellite remote sensing images over the last 30 years. Although gold cannot be seen directly by any remote sensor, the presence of minerals which form in association with this precious metal can be detected

based on their spectral signatures (Geological survey of India training Institute, Hyderabad, Government of India (2019).)

For nearly 20 years, the workhorse of mineral exploration has been Landsat Thematic Mapper/Enhanced Thematic Mapper+ (TM/ETM+), with its six spectral bands recording energy reflected by surface materials between the visible/near infrared (VNIR) and shortwave infrared

*Corresponding author. E-mail :vonjyrak@gmail.com. Tel: +261 34 46 340 46.

(SWIR) portions of the electromagnetic spectrum, plus one band in the thermal infrared (TIR).

ASTER image can map also the distribution of various minerals, including white mica, silicification, carbonates, clays, alunite and iron oxides (Rowan and Mars, 2003; Rowan et al., 2003; Hewson et al., 2005). ASTER derived mineral index maps are simple band and relative band depth ratios that correspond to absorption features for particular minerals.

The real potential for ASTER mineral index maps as an exploration tool lies in their identification of minerals distribution associated with alteration haloes and fluid flow. Walshe et al. (2003) noted that large ore deposits lie on chemical gradients such as changes in redox, pH, temperature and pressure. ASTER can identify chemical gradients preserved in the rock record as subtle variations in mineralogy (Van der Wielen et al., 2005).

In the west part of Madagascar in the Betsiriry region, they apply these techniques of image processing using ASTER and Landsat 8 images for gold prospecting. For this, the authors follow and use the different steps as follows:

- 1) Identification of the geological formation favorable for gold deposit by using index calculation
- 2) Determination of alteration zones using satellite images processing;
- 3) Identification of gold-related quartz veins (Native and sulfure-related Au deposit)

Area of interest and geology

Area of interest

The study area is located in the Dabolava town, Miandrivazo district, Menabe Region in the west part of Madagascar. Approximately it is 300 Km away from the capital Antananarivo via RN7 until Antsirabe and turn west towards the RN34 direction Miandrivazo. Geographically it is situated between longitude 45° 50 and 45° 75, latitude 19° 50 and 19° 75 with average altitude of 570m (Figure 1).

Geology

The Dabolava region is located on the western edge of the Precambrian age base of Madagascar. The basement consists of a series of metamorphosed volcano-sedimentary rocks of Proterozoic age formed by basic rocks rich in amphibolites, metagabbros and metadiorites, interstratified with quartzites, paragneiss and marbles. This series includes orthogneiss of granitic to granodioritic composition, which are in the form of porphyroid facies and potassium feldspar facies, called eyelets (centimetric lenticular eyes), and that the orthogneiss form scales within the volcano-sedimentary

series which are intersected by tourmaline pegmatitic veins and sterile gold or white quartz veins. There also appear younger plutonic suites comprising massifs of pink biotite granite with their procession of pegmatitic veins associated with Quartz, Feldspar, biotite and in addition metagabbros with local doleritic texture.

The type of gold deposit known in this region is the primary deposit belonging to the Proterozoic domain. This primary deposit is associated with the mica schist or quartzite facies of the schisto-quartzo-limestone series, transformed either by a regional metamorphism or by an intrusive contact metamorphism. It most often appears in the form of disseminated gold sulphides (Rakotoarimanana, 2001).

METHOD

The method is based on satellites images processing. They use ASTER and Landsat 8 bands for the index calculation and the identification of existing alteration minerals in the area of interest. During the study, data analyses were carried out using ENVI and ArcGIS software.

Data collection

ASTER image has 14 different spectral bands which are 3 VNIR (visible-near infrared), 6 SWIR (short wave infrared) and 5 TIR (thermal infrared) channels. Each spectral region has different spatial resolutions such as 15 m (VNIR), 30 m (SWIR) and 90 m (TIR). The most of the image processing methods use same pixel size for all channels due to pixel based arithmetic operations. In order to perform image processes, pixel size of different spectral regions of ASTER image arranged as 15m cell size for all regions by using ENVI software. This study covers only SWIR and TIR spectral region, VNIR spectral region of ASTER did not be used (Yamaguchi et al., 1998).

The ASTER image is downloaded from the website of USGS Earth Explorer and the acquisition date is 16 Mai 2015.

For this study, we use the mosaic of ASTER images AST_L1T_00309252006071532_20150516082140_22945.hdf and AST_L1T_00309252006071541_20150516082154_65354.hdf (Table 1)

Providing moderate-resolution imagery, from 15m to 100m, of Earth's land surface and polar regions, Landsat 8 operates in the visible, near-infrared, short wave infrared, and thermal infrared spectrums. Landsat 8 captures more than 700 scenes a day, an increase from the 250 scenes a day on Landsat 7. The OLI and TIRS sensors will see improved signal to noise (SNR) radiometric performance, enabling 12-bit quantization of data allowing for more bits for better land-cover characterization.

Landsat 8's Operational Land Imager (OLI) collects data from nine spectral bands. Seven of the nine bands are consistent with the Thematic Mapper (TM) and Enhanced Thematic Mapper Plus (ETM+) sensors found on earlier Landsat satellites, providing for compatibility with the historical Landsat data, while also improving measurement capabilities. Two new spectral bands, a deep blue coastal/aerosol band and a shortwave-infrared cirrus band will be collected, allowing scientists to measure water quality and improve detection of high, thin clouds.

The spatial Landsat 8 resolution of the images obtained with the TIRS instrument is 100 m. Its main purpose is to obtain surface temperature characteristics, and to study the process of heat and moisture transfer in the interests of the agricultural sector, water management, etc (Amin and Hashim , 2015).

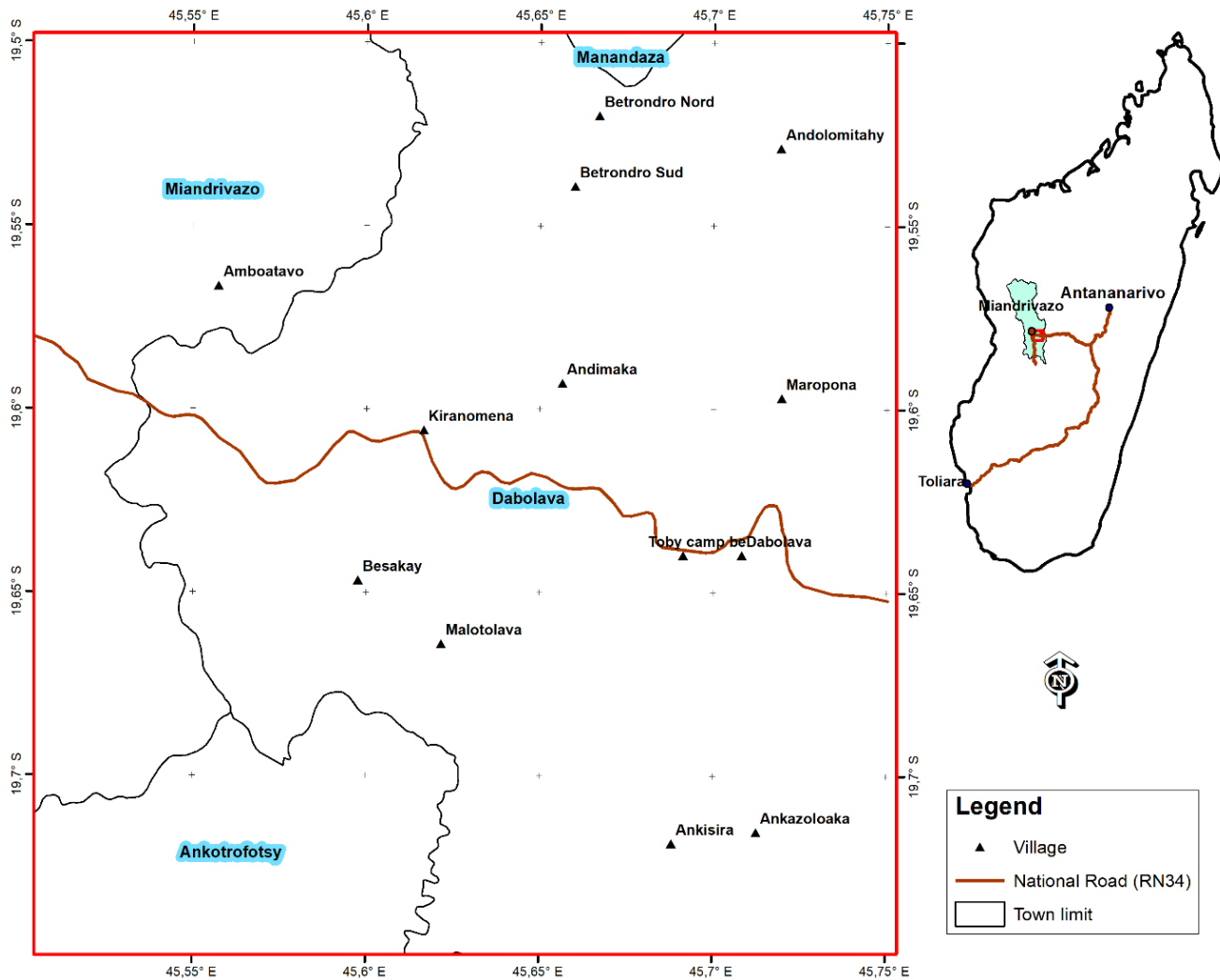


Figure 1. Localization map of the study area.

Table 1. ASTER image metadata.

Characteristic	Band	Spectral range (micrometers)	Spatial resolution (m)
VNIR	1	0.52 - 0.60	15
	2	0.63 - 0.69	
	3	0.76 - 0.86	
SWIR	4	1.60 - 0.70	30
	5	2.145 - 2.185	
	6	2.185 - 2.225	
	7	2.235 - 2.285	
	8	2.295 - 2.365	
	9	2.36 - 2.43	
TIR	10	8.125 - 8.475	90
	11	8.475 - 8.825	
	12	8.925 - 9.275	
	13	10.25 - 10.95	
	14	10.95 - 11.65	

Table 2. LANDSAT8 image metadata.

	Bands	Wavelength (µm)	Resolution (m)
Lands at 8 operational Land imager (OLI) and thermal infrared sensor (TIRS) launched February 2013	Band 1 - Coastal aerosol	0.43 - 0.45	30
	Band 2 - Blue	0.45 - 0.51	30
	Band 3 - Green	0.53 - 0.59	30
	Band 4 - Red	0.64 - 0.67	30
	Band 5 - Near infrared (NIR)	0.85 - 0.88	30
	Band 6 - SWIR 1	1.57 - 1.65	30
	Band 7 - SWIR 2	2.11 - 2.29	30
	Band 8 - Panchromatic	0.50 - 0.68	15
	Band 9 - Cirrus	1.36 - 1.38	30
	Band 10 - Thermal infrared (TIRS) 1	10.60 - 11.19	100
	Band 11- Thermal infrared (TIRS) 2	11.50 - 12.51	100

One scene of Landsat 8 image, downloaded from USGS Earth Explorer in 23 September 2020, is used during this study: LC08_L1TP_160074_20200923_20201005_01_T1 (Table 2).

DISCUSSION

Processing method

Images pre-processing

A satellite images is always exposed to several factors that disrupt to the receipt and introduces some errors in the image. To make this picture cleaner, sets of correction are applied: the geometric correction and the radiometric correction.

The geometric correction is applied to an image that distorts itself to cause of some errors in the movement of the satellite or the mechanism of receipt. In the case where there is an error on the sensors that will drive the introduction of the incorrect pixels we conducts the radiometric correction. If the cloudy cover is superior to 10% a set of stage combination is applied, it is characterized by a combination of several different dates in a same stage.

By using ENVI software, the authors conduct to the following steps. Firstly, open the image in ENVI and remove all bad data in the edge of the image. Then, group the ASTER bands by using the command "Layer stacking" and put the resolution into 15m. The next step is to combine the two ASTER image composed of the area into one image by using the "Mosaicking" command. After that, delimit the area of interest and make a color composite band. Then, calculate de NDVI (Normalized Difference Vegetation Index) and apply mask for removing the vegetation. Generally, the NDVI is given by the following formula:

$$NDVI = \frac{NIR - R}{NIR + R}$$

For ASTER image, the NDVI is:

$$NDVI = \frac{Band3 - Band2}{Band3 + Band2}$$

Or, Band3 is affected to Near Infrared and Band2 to Red

Images processing

Once the corrections are finished, we can begin the appropriate

processing of the image. In this phase, we use the color composites, the bands ratio, the raster index calculation and the topographic modeling.

Index calculation

Quartz and carbonate index

To calculate these indexes, we use TIR bands of ASTER image.

a- Quartz index

As the spectral emissivity curve of a siliceous rock shown in Figure 2b, all the silica minerals represented by the most common mineral on earth, quartz, have a unique spectral feature in thermal infrared region. That is, the silica minerals have relatively higher emissivity at 8.65 µm regions corresponding to the ASTER band 11 than at 8.3 µm regions corresponding to ASTER band 10 and at 9.1 µm region corresponding to ASTER band 12. This spectral property is applied to define QI for mapping siliceous rocks using ASTER-TIR data as (Ninomiya, 2002; Rockwell and Hofstra (2008):

$$QI = \frac{Band11 \times band11}{Band10 \times band12}$$

b- Carbonate index

The major carbonate minerals on earth, calcite and dolomite, have a unique spectral feature in thermal infrared region, as shown in Figure 2a. That is, they have an absorption feature only at 11.3 µm region corresponding to ASTER band 14. The spectral property is modified in natural cases they are mixed with other materials, however, the spectral property opposite to the one of silica and silicate minerals, which emissivity at band 14 region is less than the one at band 13 region, is usually kept. This makes sense of defining CI as (Ninomiya, 2002; Rockwell and Hofstra (2008):

$$CI = \frac{Band13}{Band14}$$

Epidote, chlorite and amphibole index

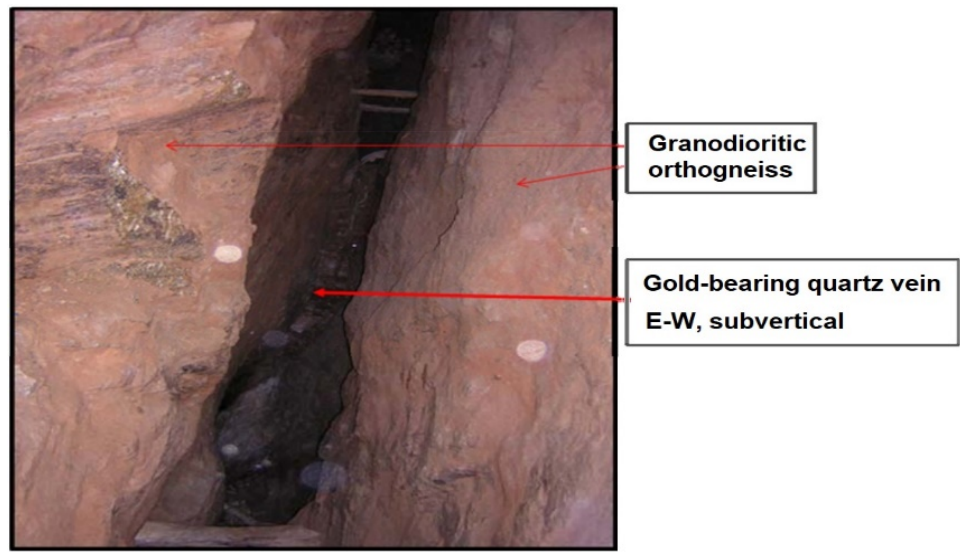
The CSIRO (Commonwealth Scientific and Industrial Research Organization) division Australia given the Aster band ratio index



a



b



c

Figure 2a. Photos. a- Large block of flush quartzite; b- Amphibolite outcrop; c- Subvertical gold-bearing Quartz vein discordant at Orthogneiss foliation (Ramiandrisoa, 2010).

(given in equation ECAI) to map the Chlorite and/or Amphibole and/or Epidote minerals is used to enhance the occurrences of these MgOH alteration and meta-volcanic alterations. The band ratio for the epidote, chlorite and amphibole minerals is defines below (Cudahy, 2012):

$$ECAI = \frac{Band6 + Band9}{Band7 + Band8}$$

Alunite and kaolinite index

To calculate this index, we use SWIR bands of ASTER image. Figure 3. shows the spectral emissivity (a)carbonate rock; (b)siliceous one; (c)felsic one; (d)intermediate one; (e)mafic one; (f)ultramafic one. Each tick in Y axis represents 1.0 or 0.5 in emissivity (Ninomiya, 2002).

Comparing the spectral reflectance curve of these minerals, 1.6

to 1.7 and 2.145 to 2.185 μm spectral regions are quite important to distinguish alunite minerals from other minerals. Similarly, 2.185 to 2.225 and 2.235 to 2.285 μm spectral regions are important for kaolinite minerals. In 1.6 to 1.7 μm and 2.145 to 2.185 μm spectral intervals are the highest reflectance and absorbance values of the alunite minerals, respectively. On the other hand, 2.235 to 2.285 μm spectral interval is the highest reflectance value of kaolinite minerals and 2.185 to 2.185 μm spectral intervals is the lowest reflectance value of the kaolinite minerals (Figure 4).

Alunite and kaolinite, which are alteration minerals present in advanced argillic alteration, have absorptions at 2.16 μm and 2.2 μm that are created by the aluminum hydroxyl (Al-OH) bond. According to Rowan (USGS, 2005), Rowan et al. (2005) this index is calculated from the following formula:

$$AKI = \frac{Band4 + Band6}{Band5}$$

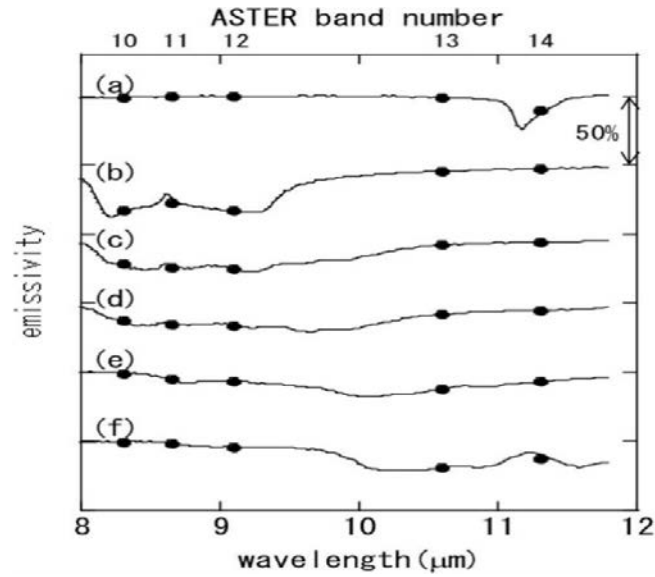


Figure 3. Spectral emissivity (a)carbonate rock; (b)siliceous one; (c)felsic one; (d)intermediate one; (e)mafic one; (f)ultramafic one. Each tick in Y axis represents 1.0 or 0.5 in emissivity (Ninomiya, 2002).

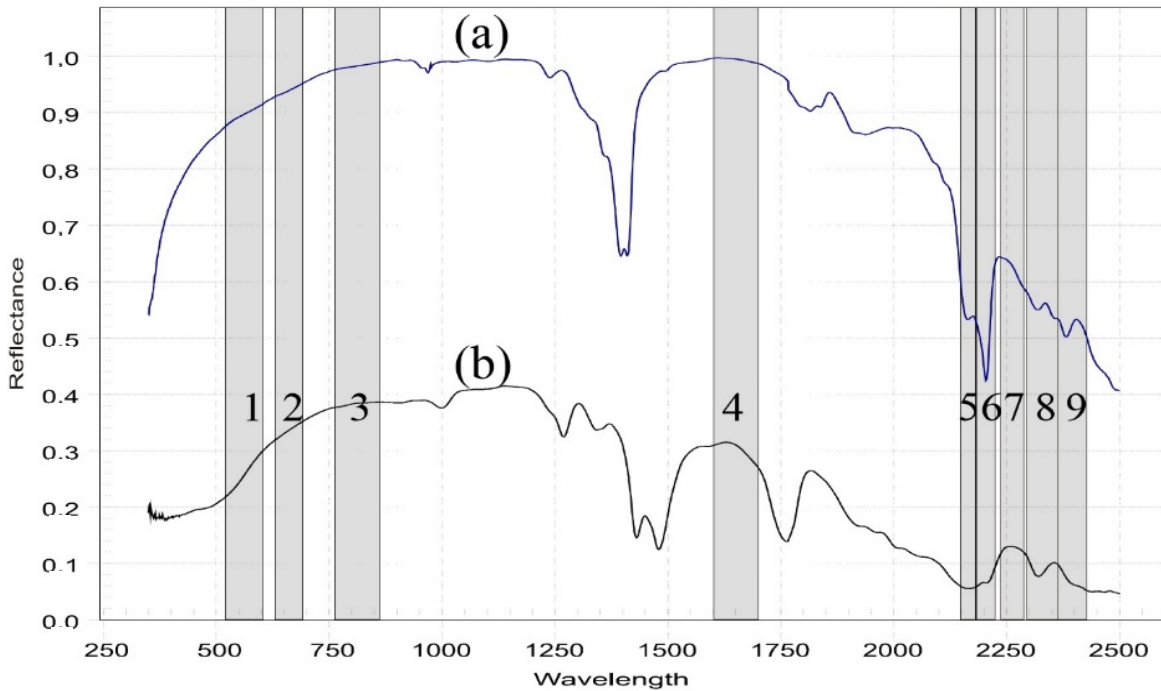


Figure 4. Spectral reflectance curves of kaolinite (a) and alunite (b) minerals within ASTER spectral channels (San et al., 2004; Yamaguchi and Takeda, 2003; Ninomiya, 2016).

Mapping

Once the processing in the ENVI software is finished, one is going to export all images toward the software of cartography for a final layout.

RESULTS AND INTERPRETATION

Here the different results of the satellite images processing are shown. The result of various index

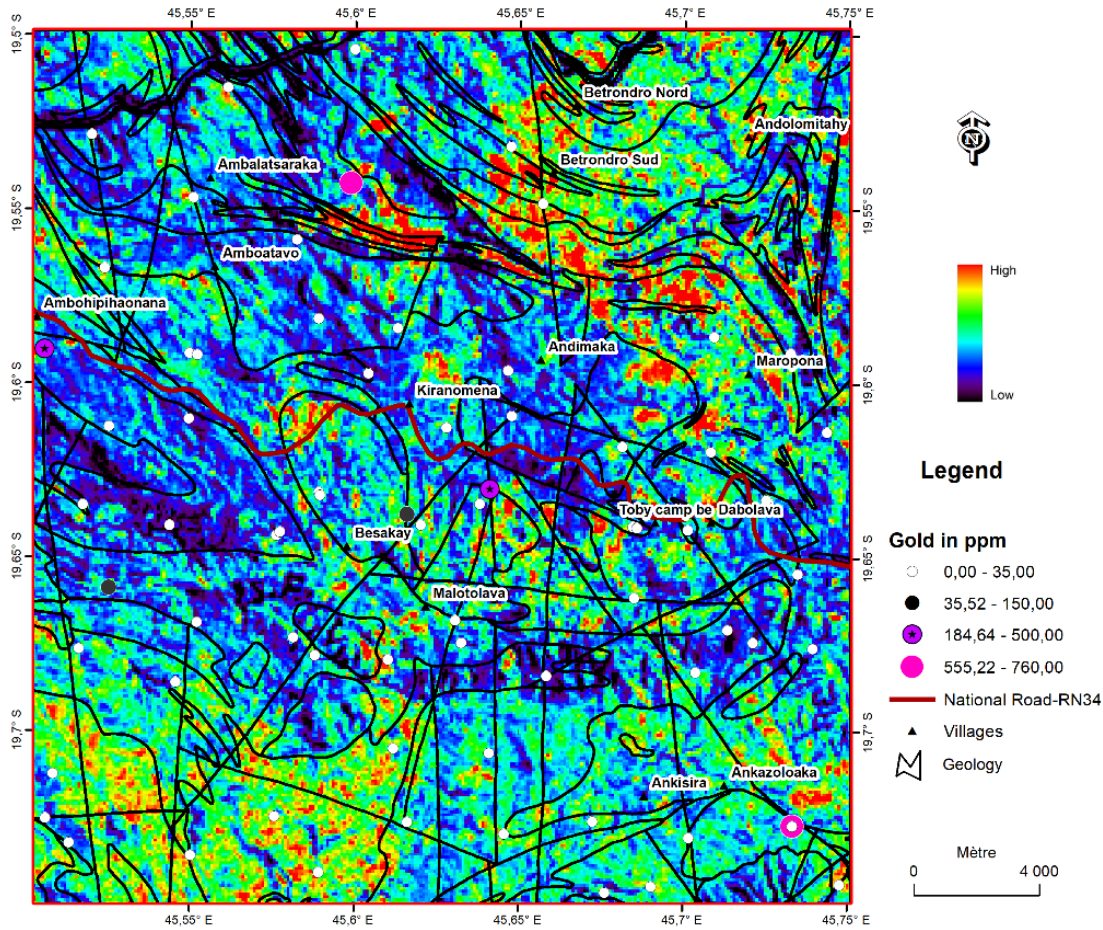


Figure 5. Quartz index.

calculation like as quartz, carbonate, epidote-chlorite-amphibole and alunite-kaolinite. There is also result of ASTER band ratio and Landsat 8 band ratio images (Annex Figures 1 to 3).

Quartz index

Quartz is a common alteration product associated with gold deposit. The use of ASTER TIR bans 10, 11 and 12 give them the result in Figure 5. The high value in Quartz is colored in Red and Orange in the map. It is associated with quartzite, amphibolite, paragneiss, clay schist, métagranodiorite, métagranite, marble and métagabbro. We can see this higher value in the northeastern and southwestern part of the study area. There is a correlation between this result and the result of geochemistry sampling.

Carbonate index

There is a big similarity between the results of quartz and

carbonate index. The high value colored in red and orange in Figure 6 is concentrated in the Northeastern and Southwestern of the region on the quartzite, paragneiss, clay schist, amphibolite, métagranite, métagranodiorite, marble and metagabbro formation.

Epidote, chlorite and amphibole index

High values of this index indicate areas that are associated with enrichment in epidote, chlorite, and amphibole minerals (red and orange colors in Figure 7).

The composite of Aster band ratio index of epidote, chlorite and amphibole give us good result. The high value is concentrated in the north and central part of the region highlighting amphibolite, métagranite, meta-granodiorite, quartzite, metagabbro, marble, paragneiss, clay schist and alluvium.

Alunite and kaolinite index

Argillic alteration is concentrated in the northwestern at

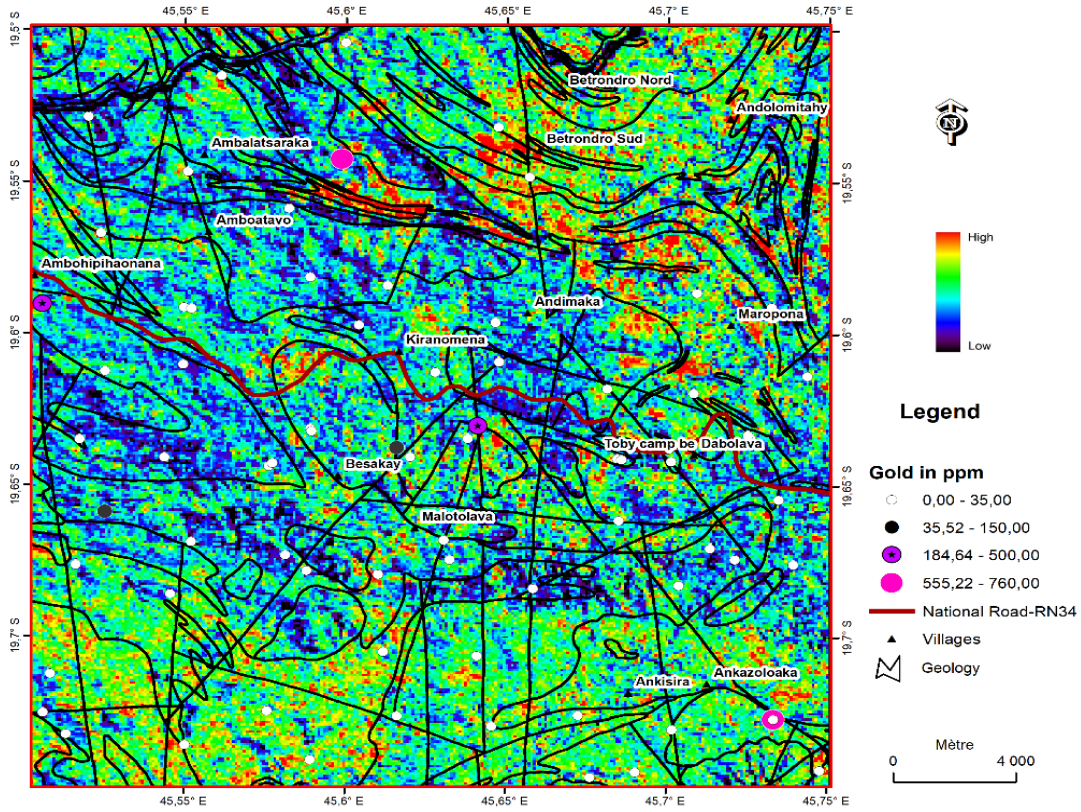


Figure 6. Carbonate index.

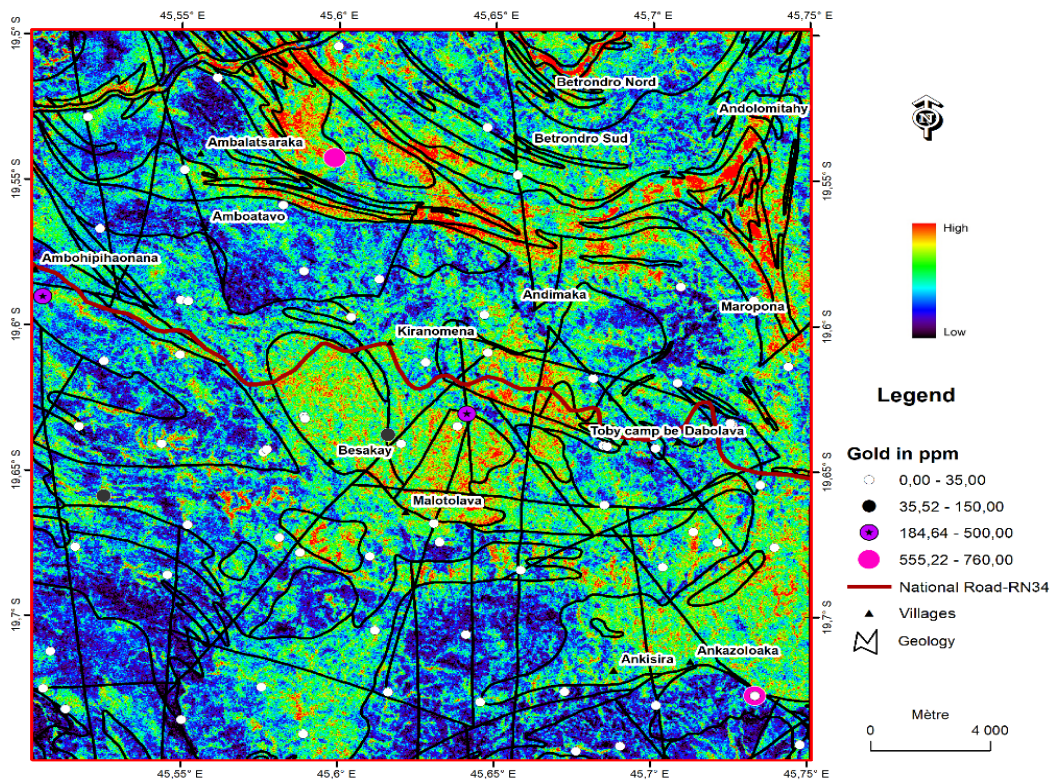


Figure 7. Epidote, chlorite and amphibole index.

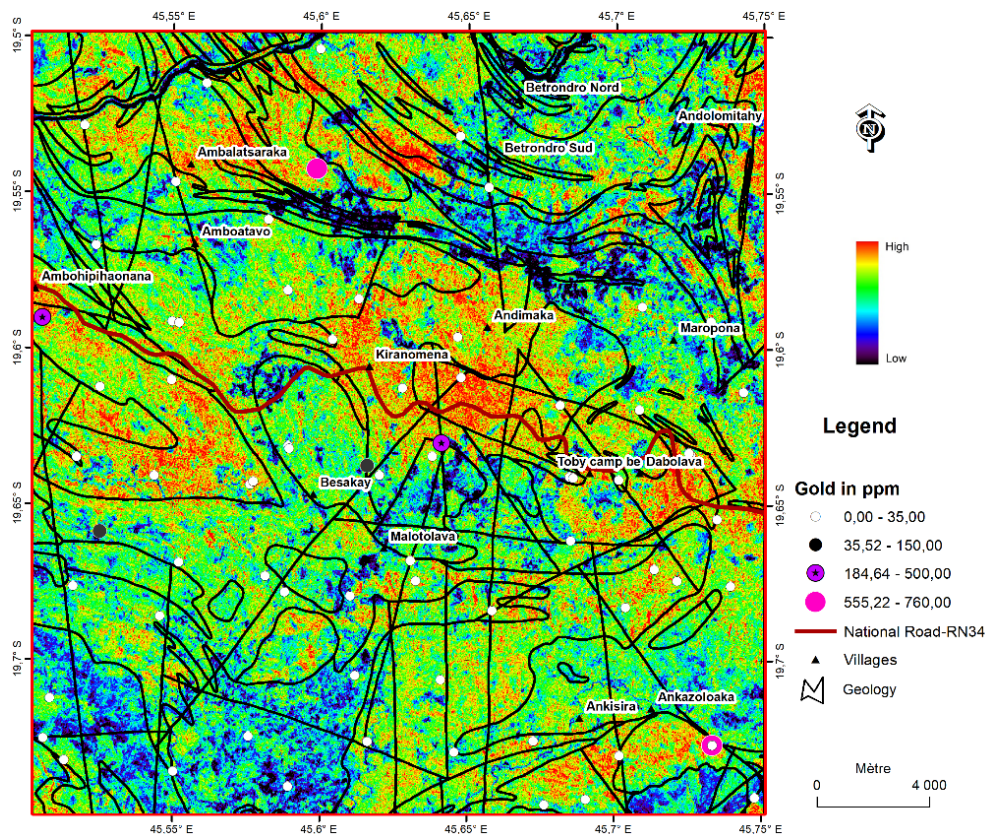


Figure 8. Alunite and kaolinite index.

Ambalatsaraka village and in the central part of the region at Kiranomena and Dabolava villages. They presents with high value on the métagranite, metagranodiorite, paragneiss, amphibolite, clay schist and marble formation.

The Figure 8 below show the distribution of argillic alteration in the region of interest.

According to the result in Figure 9 and Figure 10, the area was divided into 4 zones, following the type and degree of alteration and the overlaying geological formation. The zone A is located in the north and northeastern of the area at Ambalatsaraka to Andolomitahy throughout Betrandro Sud and Betrandro Nord villages. It is identified by the higher value in index calculation alteration. This high alteration is corresponding to the formation of amphibolite, quartzite, paragneiss, marble, clay schist and alluvium.

The zone B is delimited in the central part of the area of interest, where the national road RN34 passes. The villages inside this area are: Besakay, Kiranomena, Andimaka, Toby Camp Be, Dabolava and Maropona. The good alteration zone is related to métagabbro, métagranite, metagranodiorite, clay schist and paragneiss formation.

The zone C is situated in the southwestern part of the study area. The most important geological formation

representing the best alteration is as follows: métagabbro, métagranite, metagranodiorite and paragneiss.

The zone D characterized by the alteration in clay schist, paragneiss, métagranite, métagabbro and metagranodiorite is localized in the southeastern of the area of interest (Table 3).

ASTER RGB band combinations, band ratios and math operators have provided semi-qualitative estimations of the existing alteration and lithological units present in the study area. The ASTER TIR indices like as Quartz index and Carbonate index have a good and similar in term of result.

The alteration type with Quartz index is the silicification, which is present in the wall rock along the margins of quartz veins (Lagat, 2009). After combination of all calculation index, it can be said that the geology related to gold deposit are amphibolite, quartzite, paragneiss, clay schist, métagranodiorite, marble, metagranite, metagabbro and alluvium.

Dabolava gold deposit is stripped in the orthogneiss granodiorite age 1000 Ma or in the amphibolite age 1.9 Ga. The rock encaissant of mineralization is identified as granodiorite and gabbro from magma calco-alcalin, and amphibolite from tholeiitic. Two (02) types of deposit are identified like as: quartz veins concordant to the amphibolite-leucogneiss foliation and subvertical quartz

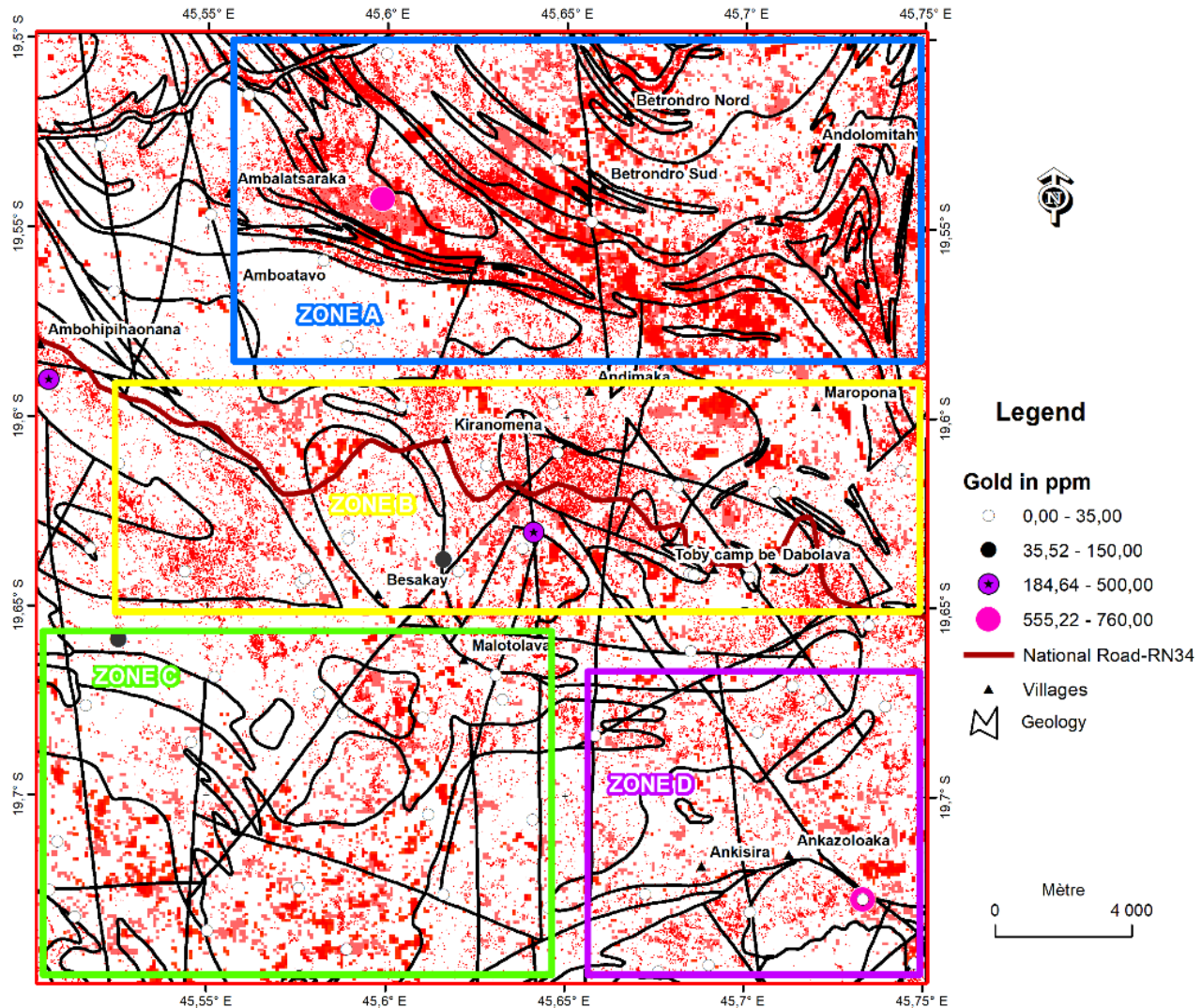


Figure 9. Superposition of all index.

Table 3. Summarize between index calculation and geology formation.

Index calculation	Geology/formation
Quartz	quartzite, paragneiss, clay schist, amphibolite, marble, métagranite, metagranodiorite and metagabbro
Carbonate	quartzite, paragneiss, clay schist, amphibolite, marble, métagranite, metagranodiorite and metagabbro
Epidote, chlorite and amphibole	amphibolite, quartzite, métagranite, metagranodiorite, metagabbro, marble, paragneiss, clay schist and alluvium
Alunite and kaolinite	Métagranite, metagranodiorite, paragneiss, amphibolite, clay schist and marble

filon discordant to the orthogneiss granodiorite (Ramiandrisoa, 2010; Ramiandrisoa et al., 2009).

Bezanahary (2005), Ndrianaly (2011) and Maminirina (2014) said in their work that the gold mineralization is associated with quartz veinlet, with more centimeter width, concordant in the general foliation of amphibolite-leucogneiss or quartz veins, 30cm to 50cm width,

discordant to orthogneiss granodiorite.

Conclusion

After analyses of ASTER images, indexes calculation and bands ratio combination show potential zone for gold

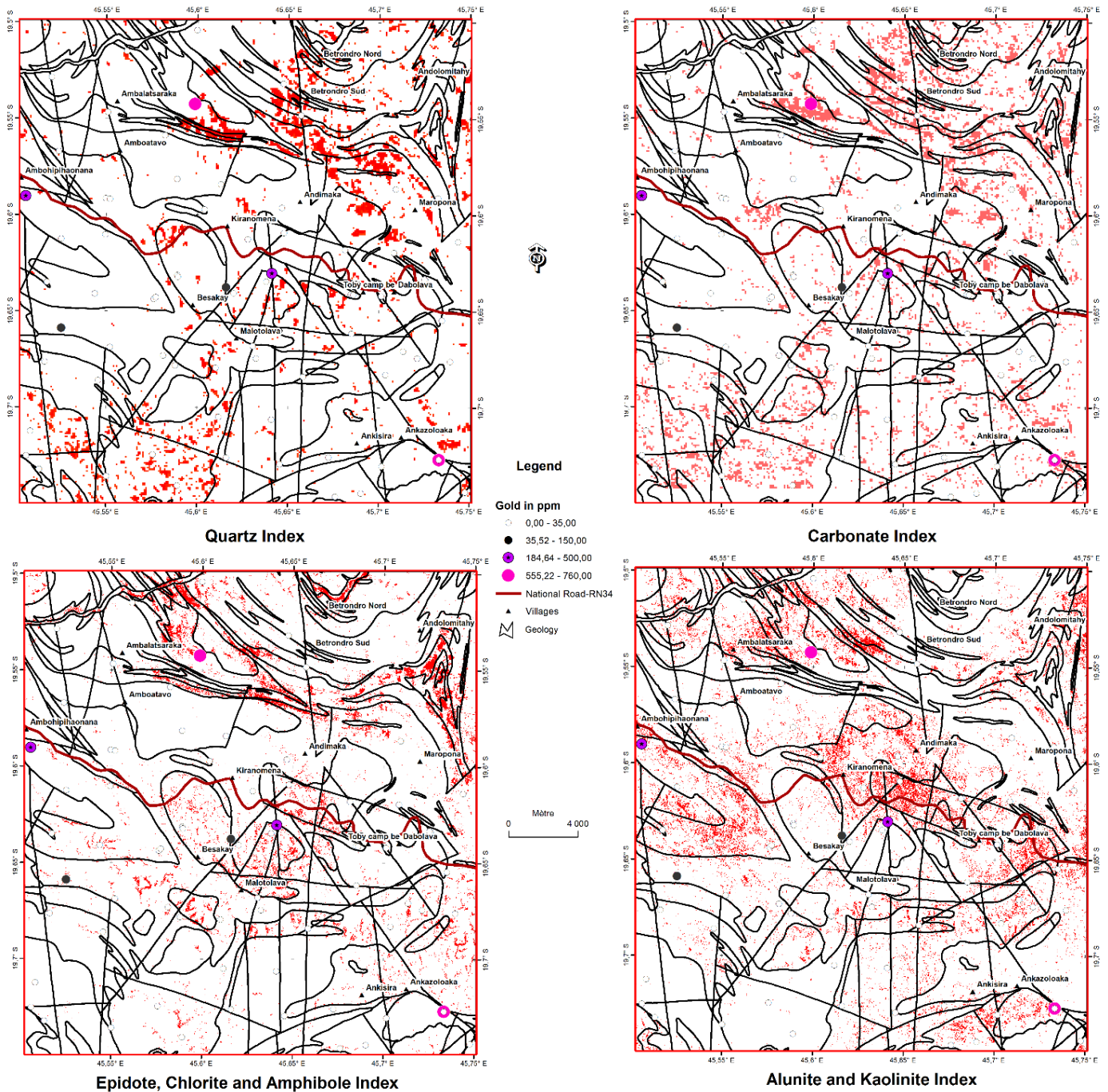


Figure 10. Summary of all indexes.

related quartz vein in the amphibolite, granodiorite, gabbro and gneiss in the study area. This result confirms the works of previous study that was by other scientists in the Dabolava region. These analyses give the authors the news shape of gold mineralization in clay schist, marble, métagranite and alluvium. After treatment and analyses of satellite images, we always recommended the field survey for verification.

CONFLICT OF INTERESTS

The authors have not declared any conflict of interests.

ACKNOWLEDGEMENTS

Special thanks go to the Ministry of Mines and Strategic

Resources of Madagascar (MMRS), Japan oil, Gas and organizing the competition of Remote Sensing in Metals National Corporation (JOGMEC), and JOGMEC Botswana Geologic Remote Sensing Centre, for SADC country members, for providing scientific data and financial research and analysis.

REFERENCES

- Amin BA, Hashim M (2015). Hydrothermal alteration mapping from Landsat-8 data, Sar Cheshmeh copper mining district, south-eastern Islamic Republic of Iran. *Journal of Taibah University for Science* 9:155-166
- Bezanahary JO (2005). Study of the Dabolava gold deposit by magnetic prospecting. Master degree from the University of Antananarivo.
- Cudahy T (2012). Satellite ASTER Geoscience Product Notes for Australia, CSIRO Earth Science and Resource Engineering EP-30-07-12-44.
- Geological survey of India training Institute, Hyderabad, Government of India (2019). Photo geology and remote sensing division. 9th course on remote sensing and digital image processing for geoscientists.
- Hewson R, Robson D, Carlton A, Gilmore P (2005). Geological application of ASTER remote sensing within sparsely outcropping terrain, Central New South Wales, Australia. *Geoinformatics*, Research article.
- Lagat J (2009). Hydrothermal alteration mineralogy in geothermal fields with case examples from Olkaria domes geothermal field, Kenya.
- Maminirina J (2014). Study of the Dabolava gold deposit using geomatics data. Master degree from the University of Antananarivo.
- Ndrinaly B (2011). Contribution of aeromagnetic data in the study of the potentiality of gold deposits in Dabolava, central western Madagascar. Mining engineer degree, University of Antananarivo-Polytechnic School of Antananarivo.
- Ninomiya Y (2002). Mapping quartz, carbonate minerals and mafic-ultramafic rocks using remotely sensed multispectral thermal infrared ASTER data. *Proceedings of SPIE* 4710:191-202.
- Ninomiya Y (2016). Lithologic mapping with multispectral ASTER TIR and SWIR data. Geological Survey of Japan, AIST.
- Rakotoarimanana RH (2001). Geology and petrology of the Dabolava region, west-central Madagascar, with emphasis on granite-hosted gold mineralization. Master in natural sciences, rand Afrikaans University 79.
- Ramiandrisoa N (2010). Metallogenic study of the Dabolava gold deposit, Western Central Madagascar - An example of mesothermal gold mineralization in Proterozoic formations. Doctoral thesis from the University of Antananarivo.
- Ramiandrisoa N, Rasolomanana E, Rabenandrasana S, Vanderhaeghe O, Andre Mayer AS, Boiron MC (2009). Gold mineralization in the Proterozoic formations of Dabolava, Miandrivazo center west of Madagascar: Petrographic and geochemical study of auriferous quartz veins, article.
- Rockwell BW, Hofstra AH (2008). Identification of quartz and carbonate minerals across northern Nevada using ASTER thermal infrared emissivity data—Implications for geologic mapping and mineral resource investigations in well-studied and frontier areas. *Geosphere* 4:218-246.
- Rowan L, Mars J, Simpson C (2005). Lithologic mapping of the Mordor, NT, Australia ultramafic complex by using Advanced Spaceborne Thermal Emission and Reflection Radiometer (ASTER). *Remote Sensing of Environment* 99:105–126.
- Rowan LC, Hook SJ, Abrams MJ, Mars JC (2003). Mapping Hydrothermally Altered Rocks at Cuprite, Nevada, Using the Advanced Spaceborne Thermal Emission and Reflection Radiometer (ASTER), a New Satellite-Imaging System. *Economic Geology* 98(5):1019-1027.
- Rowan LC, Mars J (2003). Lithologic mapping in the Mountain Pass, California area using Advanced Spaceborne Thermal Emission and Reflection Radiometer (ASTER) data. *Remote Sensing of Environment* 84(3):350-366.
- San BT, Sume EO, Gurcay B (2004). Comparison of band rationing and spectral indices methods for detecting alunite and kaolinite minerals using Aster data in Biga region, Turkey.
- Van der Wielen SE, Oliver S, Kalinowski AA, Creasy J (2005). Remotely sensed imaging of hydrothermal footprints in Western Succession, Mount Isa Inlier. In: Gibson GM & Hitchman P (eds). *pm�*CRC I1 Project Final Report—3D Basin Architecture and Minerals Systems in the Mt Isa Western Succession*. Unpublished report, 268.
- Walshe JL, Halley SW, Hall GA, Kitto P (2003). Contrasting fluid systems, chemical gradients and controls on large-tonnage, high-grade Au deposits, Eastern Goldfields Province, Yilgarn Craton, Western Australia. *Mineral Exploration and Sustainable Development, 7th Biennial SGA Meeting, Athens*, pp. 827-830.
- Yamaguchi Y, Kahle AB, Kawakami T, Paniel M (1998). Overview of the advanced spaceborne thermal emission and reflection radiometer (ASTER). *IEEE Transaction on Geoscience and Remote Sensing* 36(4):1062-1071.
- Yamaguchi Y, Takeda I (2003). Mineralogical mapping by ASTER in Cuprite, Nevada, USA. *Asian Journal of Geoinformatics* 3(3):17-24.

ANNEX

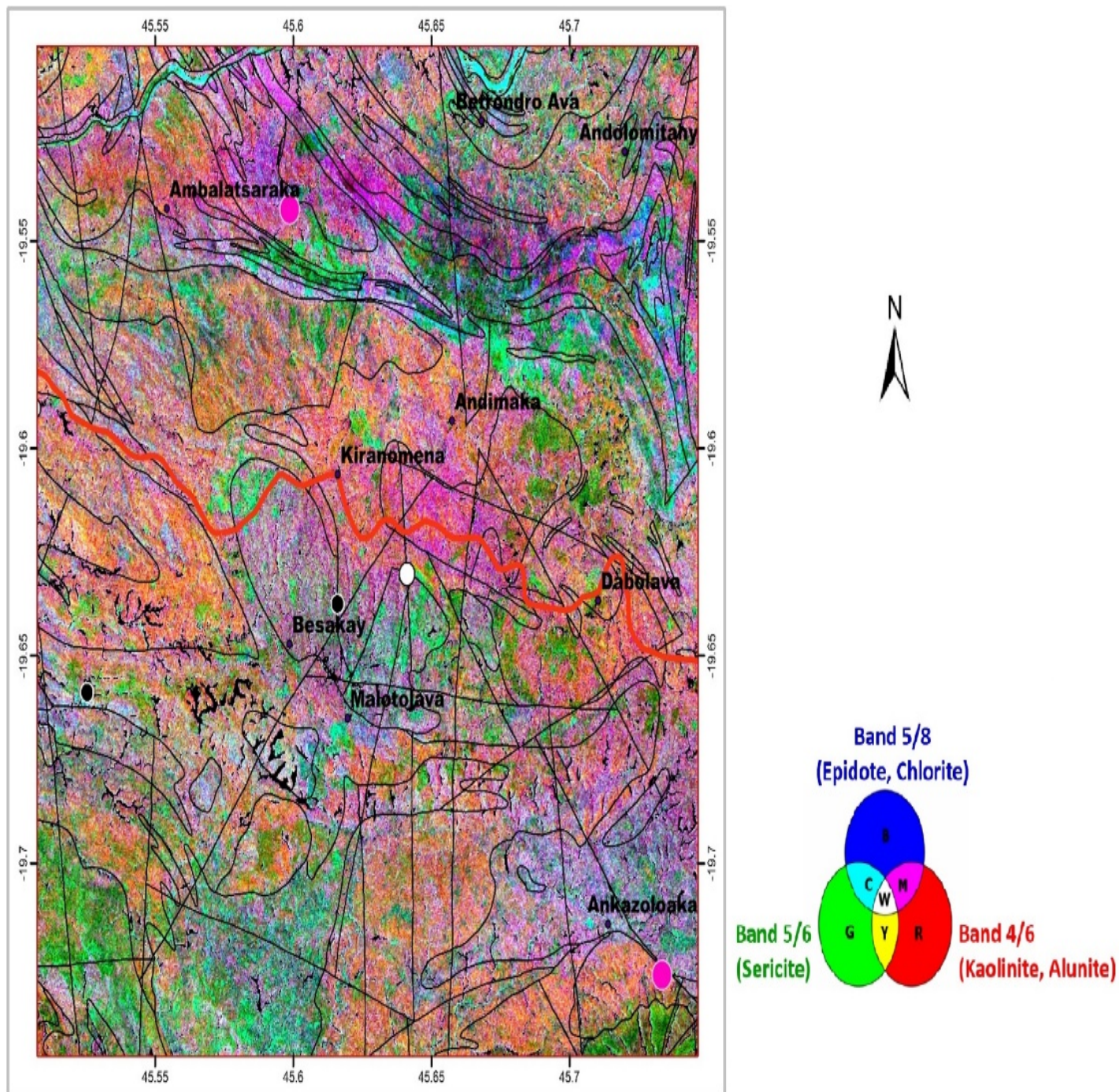
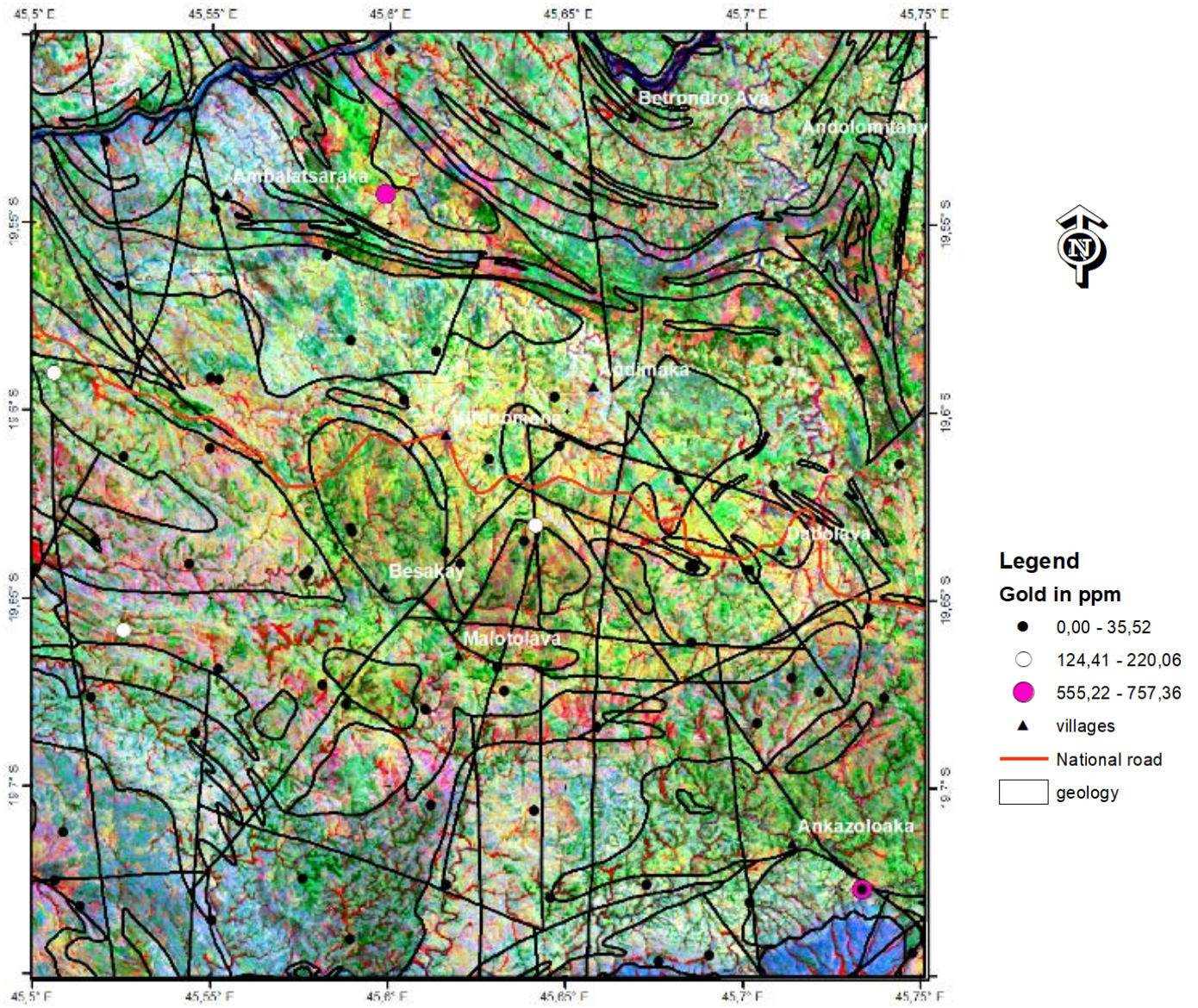
Aster band ratio

Figure 1. Band ratio image $R:G:B=B4/B6:B5/B6:B5/B8$.

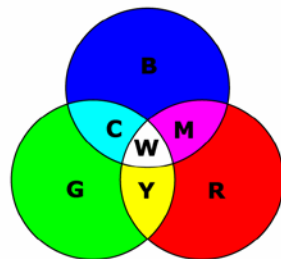
This image gives us the identification of existing alteration minerals by using an ASTER band ratio image composite of B4, B5, B6 and B8. The red color (B4/B6) show the alunite and kaolinite mineral related to advanced argillic alteration (Figure 7). The green color (B5/B6) show the sericite mineral related to phyllic alteration presents on quartzite, amphibolite, clay schist, metagranite-metadiorite, metagabbro, paragneiss. The blue (B5/B8) color show the epidote and chlorite mineral related to propylitic alteration (Figure 5).

Landsat 8 band ratio



**Band 4/2: iron oxide
(Hematite)**

**Band 6/5: iron
(Goethite, Limonite)**



(Kaolinite, Smectite)

Figure 2. Chica-Olmo band ratio.

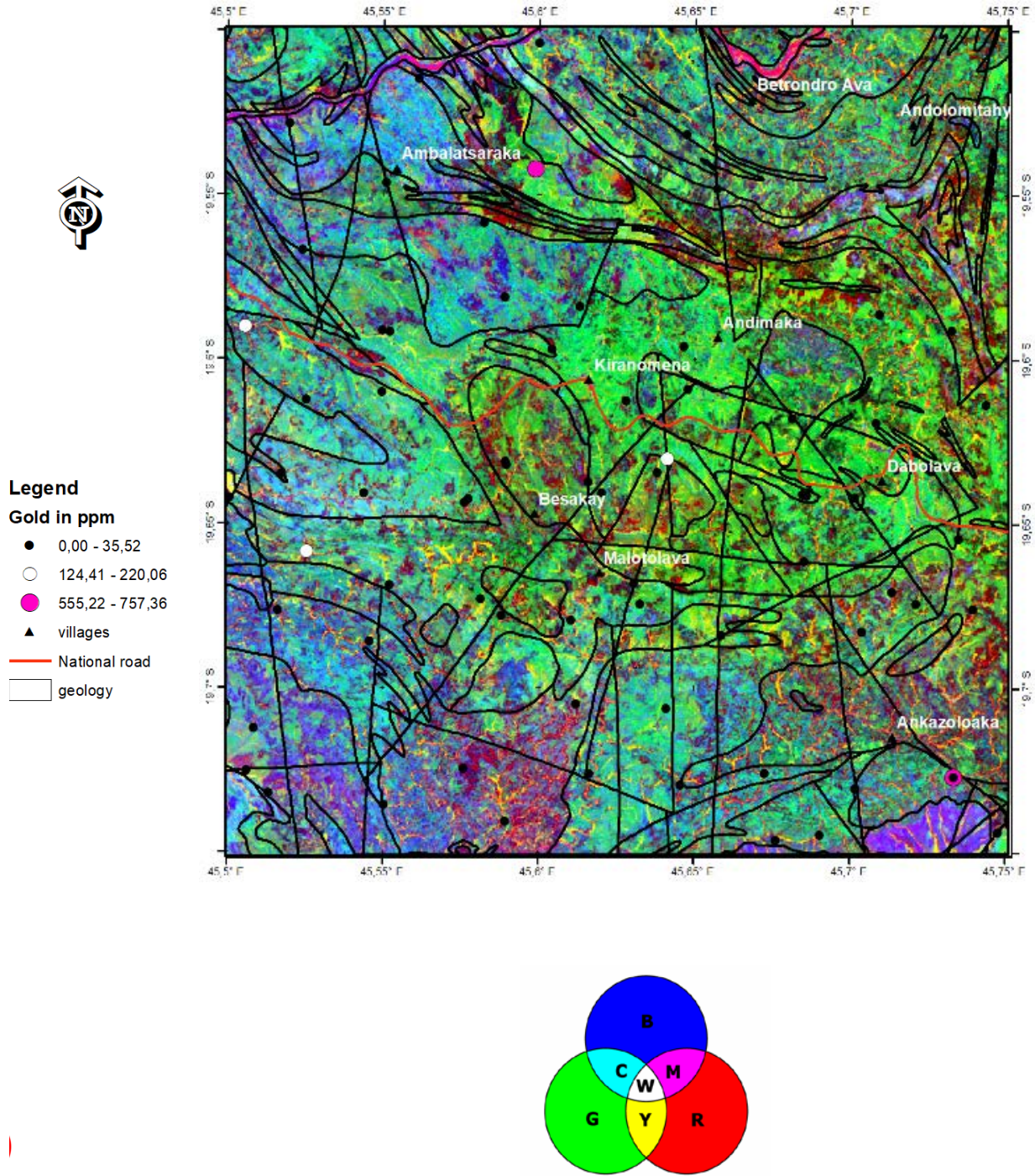


Figure 3. Band ratio $R:G:B=B5/B6:B6/B7:B2$.

Annex Figure 1 shows the result of Chica-Olmo band ratio. The ratio of B6/B7 give the existing clay minerals colored in red or pink like smectite and kaolinite. The ratio of B6/B5 show the iron minerals colored in green or cyan color such as goethite and jarosite expected hematite. The ratio of B4/B2 give iron oxide colored in blue.cyan including hematite. In 2017, Safari et al. developed a band ratio by using three bands of Landsat8 images.

Annex Figure 2 and 3 give the result of this band ratio composed by B2, B5, B6 and B7. For that B5/B6 is affected to Red, B6/B7 affected to Green and B2 affected to Blue. The result of B5/B6 ratio is colored as red. For B6/B7 ratio, the result is seen as green color. Band 2 give the existing alteration colored in blue.